

GAZİ

JOURNAL OF ENGINEERING SCIENCES

## Gyroscopic Vibration Damper for One-Storey Building: Theoretical and Experimental Research

Faruk Ünker<sup>a</sup>, Olkan Çuvalcı<sup>b</sup>

Submitted: 09.09.2022 Revised: 21.11.2022 Accepted: 03.12.2022 doi:10.30855/gmbd.0705034

### ABSTRACT

**Keywords:** Vibration control, gyroscope, gyrostabilizer, vibration absorbers, nonlinear dynamics, damping

<sup>a</sup> Gümüşhane University, Faculty of Engineering, Dept. of Mechanical Engineering, 29100 - Gümüşhane, Türkiye  
Orcid: 0000-0002-9709-321X  
e mail: farukunker@gumushane.edu.tr

<sup>b</sup> Karadeniz Technical University, Faculty of Engineering, Dept. of Mechanical Engineering, 61080 - Trabzon, Türkiye  
Orcid: 0000-0001-8596-5941

\*Corresponding author:  
farukunker@gumushane.edu.tr

In this study, a gyroscopic damper model consisting of a built-in column has been developed. The objective of this study is determining the required angular momentum with the optimum ratio of natural frequency for the gyroscopic vibration absorber under sinusoidal excitation. This damper model is investigated experimentally and theoretically for different angular momentums of the gyroscope and different frequency ratios of the structure and damper on a single-story structure. As a result of the study, the displacement of the structure at the 1st mode frequency for a given angular momentum of the gyroscope is fairly reduced. Besides, at a notable frequency ratio of the damper and the structure, the effect of the angular momentum is improved. Even if the disk mass of the gyroscope decreases, it is possible to obtain a certain angular momentum by increasing the disk speed. Thus, lighter and less bulky gyroscopic vibration dampers can be designed. The cooperation of the required angular momentum with the optimum ratio of natural frequencies should be considered to obtain a highest attenuation of the building vibration. In addition, the equations of motion obtained according to the 1st mode and the theoretical results overlapped.

## Bina için Jiroskopik Titreşim Sönümleyici: Teorik ve Deneysel Araştırma

### ÖZ

Bu çalışmada, kolon üzerine bağlanmış bir jiroskopik sönümleyici modeli üzerine çalışılmıştır. Bu çalışmanın amacı, sinüzoidal zorlayıcı yük altında jiroskopik titreşim sönümleyici için gerekli açısız momentum ile optimum doğal frekans oranı belirlenmesidir. Bu sönümleyici modeli, tek katlı bir yapı üzerinde jiroskopun farklı açısız momentumları ve yapı ile sönümleyicinin farklı frekans oranları için deneysel ve teorik olarak incelenmiştir. Çalışma sonucunda, jiroskopun belirli bir açısız momentumu için yapının 1. mod frekansında yer değiştirmesi oldukça azaltılmıştır. Ayrıca, sönümleyici ve yapının belli bir frekans oranında açısız momentumun etkisi iyileşmiştir. Jiroskopun disk kütlesi azalsa dahi disk hızını artırarak belirli bir açısız momentum elde etmek mümkündür. Böylece daha hafif ve daha az hacimli jiroskopik titreşim sönümleyici tasarlanabilir. Bina titreşiminde en yüksek sönümleme elde etmek için, gerekli açısız momentumun ile optimum doğal frekans oranı ile bağlantısı hesaba katılmalıdır. Ayrıca 1. moda göre elde edilen hareket denklemleri ile teorik sonuçlar örtüşmüştür.

**Anahtar Kelimeler:** Titreşim kontrolü, jiroskop, jirostabilizer, titreşim yutucu, doğrusal olmayan dinamikler, sönümleme

## 1. Introduction

In conditions where the natural frequency of the main building is very close to the frequency band of the force forcing this building, resonance that causes large displacements occurs [1]. Dynamic dampers are sub-systems that absorb most of the energy of the main structure by transferring them to prevent resonance [2], [3]. Dynamic dampers are generally evaluated in three categories: passive, active, and hybrid. Until today, many dynamic dampers, both passive and active, that can meet external loads such as earthquakes and wind, have been applied to various structures [4].

Passive vibration dampers do not need external energy to dampen. On the contrary, they get their kinetic energy from the movement of the structure to be damped [1]. These systems are low cost as they do not require extra energy and actuator to dampen the main structure. Passive dampers are preferred due to their low cost and simple technology. However, passive vibration dampers need the vibration (displacement) of the structure to be damped to work [1]. This causes the system to work late and act dependent on the main structure. In passive control methods, the system cannot respond to variable vibration loads because the damper is adjusted according to the resonance region of the main structure [1]–[3].

Active dampers consist of sensors that measure the vibrations affecting the structure and computer that analyses the measured data from the sensors, and actuators that generate the necessary control forces according to the analysis obtained [2]–[4]. It can always respond quickly to changing external effects in active control methods. However, the technology used in active control systems is costly and requires large-scale external energy [2], [3]. There are negative situations in both active and passive vibration dampers. Therefore, to get rid of the disadvantages of both types of dampers, hybrid dampers have been developed in which both dampers are used together [1]–[4].

Today, gyroscopic stabilizers are widely researched in different fields [5]–[12]. In its simplest form, the gyroscope consists of a rotating disk around a certain axis and a gimbal in which the disk is placed. Active control moment gyro is more effective in damping vibration, although a passive gyroscope gives better results in terms of energy consumption. Compared to conventional active mass dampers, using gyroscopic vibration dampers to reduce vibrations provides weight and volume savings. In another study, Ünker and Çuvalcı [5] theoretically investigated the effect of gyroscopic vibration dampers in flexible structures under seismic effects and showed that the amount of bending of the flexible structure decreased. Çuvalcı et al. [6] investigated the gyroscopic vibration damper as a passive vibration damper in a 0.5-meter beam under the effect of harmonic load. In this theoretical and experimental study, the equations of motion are derived from the energy equations of the beam and the control moment gyroscope with the help of the Lagrangian method. The analysis of the equations of motion of the system is simplified to ordinary differential equations by using the first mode (effective mode) approach. In their numerical studies, they observed that the gyroscopic vibration damper effectively absorbs the vibrations of the cantilever beam. Ünker [9]–[11] also examined the control moment gyroscope in terms of dynamics and control of vehicle systems. Thanks to the gyroscopes he applied to the two-wheeled robot, he managed to keep the balance of the robot stable and under constant load [9]. In his work, he also derived the optimum velocity relation by applying certain harmonic functions to the equations of motion. Thanks to the control torques applied by the gyroscopes to the gimbal, it not only eliminated the reaction forces but also kept the robot's body in balance with a very small oscillation. In another study, Ünker [10] theoretically examined the gyroscopic stabilizer on a heavy-duty vehicle. Soleymani and Norouzi [12] theoretically investigated the gyroscopic damper they developed to dampen the vibrations on the multi-megawatt wind turbine and they succeeded in increasing the damping effect of the gyroscope by using a controller. The most important advantage of this active gyro damper is that a PID and Fuzzy controlled torque is applied externally to the gyroscope's gimbal to control the gyroscope's angular momentum. According to the results obtained, the control moment gyroscope has shown that the classical linear dampers can perform all their duties, recover faster, and operate at wide damping ratios. It has also shown that, like the two-wheeled robot, the truck trailer can remain in balance under constant and continuous load without external support. In addition to being used as a control moment gyroscope vibration damper, it can also be used as a stabilizer under a constant and continuous load without the help of any external force.

This research, it is aimed to dampen a single-storey structure by using the angular momentum of the gyroscope, which is designed as a hybrid damper. In its simplest form, the gyroscope consists of a rotor

that rotates in a ball bearing. The most important parameter of the gyro motion is based on the conservation rule of angular momentum [1]. Therefore, even if the rotor mass of the gyroscope decreases, its angular momentum can be increased if the rotor speed is increased. Thus, lighter and less bulky dampers can be designed compared to conventional dampers. For the theoretical and experimental research of the gyroscope vibration damper on a single-storey structure, the gyroscope-bearing recessed column model was used. In the theoretical research, the motion equations of the system (partial differential equations) were obtained by substituting the kinetic and potential energy equations describing the main structure and the damper in the Lagrangian equation. The obtained equations of motion are simplified to ordinary differential equations with integral constants by using the first mode approach.

## 2. Model Set-Up Design

The schematic model of the test setup is shown in Figure 1. The single-storey building in the experimental setup basically consists of two main parts. The first part consists of a gyroscope and a flexible steel column that carries the gyroscope and rises from the upper block of the building. The second part is a single-story structure, which consists of four flexible columns carrying the upper block, fixed from the other end to the lower block (ground of the lower floor). The floor plate of the single-story building is mounted by sitting on two parallel liner slides so that the desired displacement movement can only be made in the horizontal direction. All other physical data of the test model are given in Table 1. As seen in Figure 1, the motion coming from the shaker with a certain frequency and amplitude is transmitted horizontally to the floor of the single-story building model. The displacement amplitudes of the shaker and the frequency increment control in scanning were performed using the Brüel & Kjaer / LDS CometUSB vibration controller. In all experimental and theoretical studies, harmonic acceleration, linear scanning type, and 0.001 Hz/second increment rate were selected and kept constant.

In Figures 1 and 2, an aluminum plate with mass of  $M_{2t}$  is attached to the free end of four vertical cantilever beams at length of  $L_2$ . All those the other end of the beams are fixed to the aluminum base plate that is attached to the shaker with solid metal lever. Therefore, the base plate of the one story building's test model excites by shaker harmonically with varying forcing frequencies ( $\omega$ ) and amplitudes ( $z_0$ ) by the base excitation of  $z = z_0 \cos(\omega t)$ . Beams are initially assumed straight and beams horizontal and vertical displacements are also assumed elastic.

Table 1. Physical properties of the test model [8]

<i>Symbol</i>	<i>Model values</i>	<i>Model Descriptions</i>
$\rho$	7850 kg/m <sup>3</sup>	Steel density
$z_0$	0.005 m	Excitation amplitude
$E$	210e9 N/m <sup>2</sup>	Young's modulus
$L_1$	0.14 m	Length of the gyro carrier beam
$L_2$	0.20 m	Height of the one-story building
$M_1$	0.65 kg	Tip mass of the gyro carrier beam
$M_2$	2.75 kg	Tip mass of the one-story building
$m_f$	0.311 kg	Mass of the gimbal
$I_1$	2.5333e-11	Mass moment of inertia of gyro beam
$I_2$	3.3667e-11	Mass moment of inertia of storey
$I_t$	1e-2 kg.m <sup>2</sup>	Tip mass moment of gyro-beam inertia
$I_{2t}$	12e-2 kg.m <sup>2</sup>	Tip mass moment of storey inertia
$A_1$	7.6000e-5 m <sup>2</sup>	Area of gyro beam
$A_2$	1.7600e-4 m <sup>2</sup>	Total area of storey beams
$R$	0.04 m	Centroid radius of the gimbal
$g$	9.81 m/s <sup>2</sup>	Gravitational acceleration
$k_g$	0 N.m /rad	Torsion spring stiffness of gyro
$c_g$	0.0005 N.m.s/rad	Damper coefficient of gyro
$m$	0.023-0.115 kg	Disk mass
$r$	0.05 m	Disk radius
$I_p$	(mr <sup>2</sup> )/2+2.66e-5 kg.m <sup>2</sup>	Disk's rotary inertia
$I_o$	(mr <sup>2</sup> )/4 kg.m <sup>2</sup>	Disk inertia of mass moment
$I_{fx}$	6.74 e-4 kg.m <sup>2</sup>	Gimbal inertia of mass moment
$I_{fy}$	6.29 e-4 kg.m <sup>2</sup>	Gimbal inertia of mass moment
$I_{fz}$	3.60 e-4 kg.m <sup>2</sup>	Gimbal inertia mass moment
$\Omega$	0-10000 rpm	Disk rotating speed

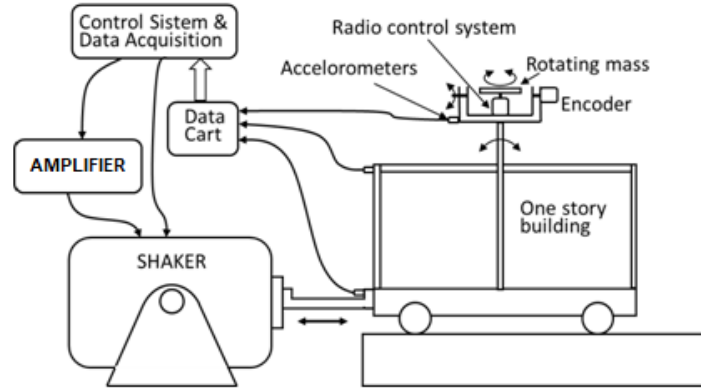


Figure 1. Experimental set-up [8]

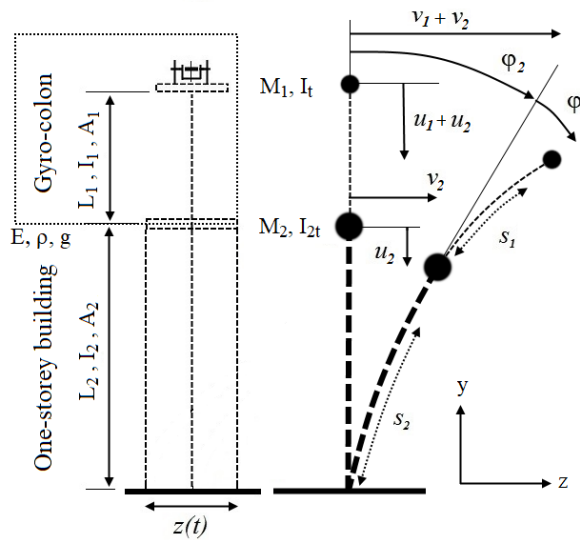


Figure 2. One-Storey building mathematical model [8]

2.1. Mathematical Model

The horizontal displacements of gyro-beam and one-storey building at the free end represent by  $v_1$  and  $v_2$ , respectively. Here,  $s_n$  indicates the extent along the arc-length of the column because of elastic deformation of the column (where  $n=1,2$ ). The gyro beam absorber consists of rotating mass (disk) that is attached to the gimbal through the electrical motor are mounted to top of flexible beam as seen in Figure 2. The rotating disk mass and disk angular velocity are represented with  $m$  and  $\Omega$  respectively. The orientation angle of the beam was given as [13]-[15].

$$\phi(s_n, t) = \sin^{-1} v'_n \approx v'_n + \frac{1}{6} v_n'^3 \tag{1}$$

Since tip masses of test model are significantly larger than the beam masses, the beam deflection can be expressed with the following shape function for the first mode,  $\psi(s_n)$  [16].

$$v(s_n, t) = v(t)\psi(s_n) \tag{2}$$

Where,

$$\psi(s_n) = 1 - \cos\left(\frac{\pi s_n}{2L_n}\right) \tag{3}$$

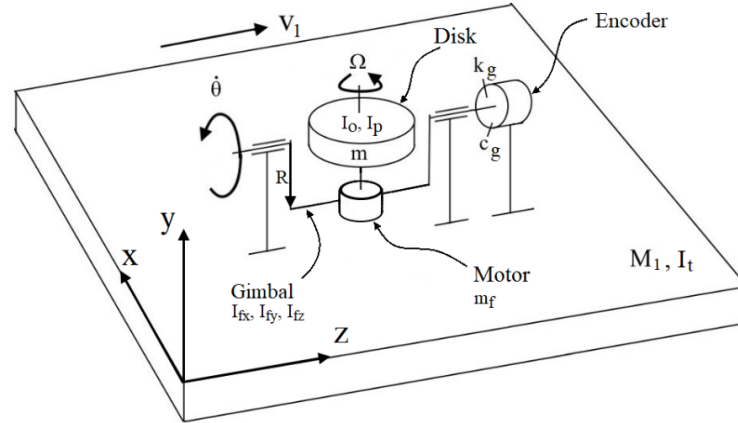


Figure 3. Gyro model with the encoder [8]

By using Lagrange's equation then making some mathematical manipulations, equations of motion of the gyro-column, the single-storey, and gyroscope at the free end are obtained as follow respectively [8]

$$\begin{aligned} & \left[ C_1 + C_2 v_1^2 + C_3 v_1^4 + \left( \frac{(I_p + I_{fy}) \sin^2 \theta}{+(I_o + I_{fx}) \cos^2 \theta} \right) \left( G_5 + \frac{1}{2} v_1^2 G_5^3 \right)^2 \right] \ddot{v}_1 \\ & + \left[ C_2 + 2C_3 v_1^2 + G_5^3 \left( \frac{(I_p + I_{fy}) \sin^2 \theta}{+(I_o + I_{fx}) \cos^2 \theta} \right) \left( G_5 + \frac{1}{2} v_1^2 G_5^3 \right) \right] v_1 \dot{v}_1^2 \\ & + \left\{ C_4 + C_5 v_1^2 + C_6 v_1^4 + C_7 (v_2 \ddot{v}_2 + \dot{v}_2^2) \right. \\ & \left. + \frac{1}{2} I_t \left[ \ddot{v}_2 G_{15} + \frac{1}{2} v_2 (v_2 \ddot{v}_2 + 2\dot{v}_2^2) G_{15}^3 \right] G_5^3 v_1 \right\} v_1 \\ & + \left. \left\{ \begin{aligned} & \left( \frac{I_{fy} - I_{fx}}{+I_p - I_o} \right) \left[ \left( G_5 + \frac{1}{2} v_1^2 G_5^3 \right) \dot{v}_1 \right. \\ & \left. + \left( G_{15} + \frac{1}{2} v_2^2 G_{15}^3 \right) \dot{v}_2 \right] \dot{\theta} \sin 2\theta \\ & + \left( \frac{(I_o + I_{fx}) \cos^2 \theta}{+(I_p + I_{fy}) \sin^2 \theta} \right) \left[ \ddot{v}_2 G_{15} + \frac{1}{2} v_2 (v_2 \ddot{v}_2 + 2\dot{v}_2^2) G_{15}^3 \right] \left( G_5 + \frac{1}{2} v_1^2 G_5^3 \right) \\ & + I_p \Omega \dot{\theta} \cos \theta \end{aligned} \right\} \left( G_5 + \frac{1}{2} v_1^2 G_5^3 \right) \tag{4} \\ & = -\gamma_1 (\ddot{v}_2 + \ddot{z}) - I_t \left[ \ddot{v}_2 G_{15} + \frac{1}{2} v_2 (v_2 \ddot{v}_2 + 2\dot{v}_2^2) G_{15}^3 \right] G_5 \end{aligned}$$

$$\begin{aligned}
 & \left[ C_8 + C_9 v_2^2 + C_{10} v_2^4 + \left( \frac{(I_p + I_{fy}) \sin^2 \theta}{+(I_o + I_{fx}) \cos^2 \theta} \right) \left( G_{15} + \frac{1}{2} v_2^2 G_{15}^3 \right)^2 \right] \ddot{v}_2 \\
 & + \left[ C_9 + 2C_{10} v_2^2 + G_{15}^3 \left( \frac{(I_p + I_{fy}) \sin^2 \theta}{+(I_o + I_{fx}) \cos^2 \theta} \right) \left( G_{15} + \frac{1}{2} v_2^2 G_{15}^3 \right) \right] v_2 \dot{v}_2^2 \\
 & + \left\{ \begin{aligned} & C_{11} + C_{12} v_2^2 + C_{13} v_2^4 + C_7 (v_1 \ddot{v}_1 + \dot{v}_1^2) \\ & + \frac{1}{2} I_t \left[ \ddot{v}_1 G_5 + \frac{1}{2} v_1 (v_1 \ddot{v}_2 + 2\dot{v}_1^2) G_5^3 \right] G_{15}^3 v_2 \end{aligned} \right\} v_2 \\
 & + \left\{ \begin{aligned} & \left( \frac{I_p - I_o}{+I_{fy} - I_{fx}} \right) \left[ \begin{aligned} & \dot{v}_1 \left( G_5 + \frac{1}{2} v_1^2 G_5^3 \right) \\ & + \dot{v}_2 \left( G_{15} + \frac{1}{2} v_2^2 G_{15}^3 \right) \end{aligned} \right] \dot{\theta} \sin 2\theta \\ & + \left( \frac{(I_p + I_{fy}) \sin^2 \theta}{+(I_o + I_{fx}) \cos^2 \theta} \right) \left[ \begin{aligned} & \ddot{v}_1 G_5 + \frac{1}{2} v_1 (v_1 \ddot{v}_1 + 2\dot{v}_1^2) G_5^3 \end{aligned} \right] \left( G_{15} + \frac{1}{2} v_2^2 G_{15}^3 \right) \\ & + I_p \Omega \dot{\theta} \cos \theta \end{aligned} \right\} \left( G_{15} + \frac{1}{2} v_2^2 G_{15}^3 \right) \tag{5} \\
 & = -\gamma_1 \ddot{v}_1 - \gamma_2 \ddot{z} - I_t \left[ \ddot{v}_1 G_5 + \frac{1}{2} v_1 (v_1 \ddot{v}_1 + 2\dot{v}_1^2) G_5^3 \right] G_{15}
 \end{aligned}$$

$$\begin{aligned}
 & (I_o + I_{fx}) \ddot{\theta} - \frac{1}{2} \left[ \begin{aligned} & \dot{v}_1 \left( G_5 + \frac{1}{2} v_1^2 G_5^3 \right) \\ & + \dot{v}_2 \left( G_{15} + \frac{1}{2} v_2^2 G_{15}^3 \right) \end{aligned} \right]^2 (I_{fy} - I_{fx} + I_p - I_o) \sin 2\theta \\
 & - \left[ \begin{aligned} & \dot{v}_1 \left( G_5 + \frac{1}{2} v_1^2 G_5^3 \right) \\ & + \dot{v}_2 \left( G_{15} + \frac{1}{2} v_2^2 G_{15}^3 \right) \end{aligned} \right] I_p \Omega \cos \theta + k_g \theta + c_g \dot{\theta} + m_f g R \sin \theta = 0 \tag{6}
 \end{aligned}$$

Where,

$$C_1 = M_1 + I_t G_5^2 + \rho A_1 G_1$$

$$C_2 = \rho A_1 G_3 + I_t G_5^4 + M_1 G_4^2$$

$$C_3 = \frac{1}{4} I_t G_5^6$$

$$C_4 = -M_1 g G_4 + E I_1 G_6 - \rho A_1 g G_9$$

$$C_5 = 2EI_1G_7$$

$$C_6 = \frac{3}{4}EI_1G_8$$

$$C_7 = \rho A_1 G_9 G_{14} + M_1 G_4 G_{14}$$

$$C_8 = \rho A_1 L_1 + \rho A_2 G_{11} + M_1 + M_2 + (I_t + I_{2t}) G_{15}^2 \quad (7)$$

$$C_9 = \rho A_2 G_{13} + (M_1 + M_2) G_{14}^2 + \rho A_1 G_{14}^2 + (I_t + I_{2t}) G_{15}^4$$

$$C_{10} = \frac{1}{4} G_{15}^6 (I_t + I_{2t})$$

$$C_{11} = EI_2 G_{16} - \rho A_1 g G_{14} L_1 - \rho A_2 g G_{19} - (M_1 + M_2) g G_{14}$$

$$C_{12} = 2EI_2 G_{17}$$

$$C_{13} = \frac{3}{4} EI_2 G_{18}$$

$$\gamma_1 = \rho A_1 G_2 + M_1$$

$$\gamma_2 = \rho A_1 L_1 + \rho A_2 G_{12} + M_1 + M_2$$

$z$  is the base displacement of one storey building ( $z = z_0 \cos(\omega t)$ ). By putting zero into equation (4), (5) and (6) for  $\dot{v}_1, \dot{v}_2 \approx 0$  and  $\dot{\theta} \approx 0$ , the equations are reduced. Assume  $\theta=0$  for small vibrations. Respectively, the natural frequencies of gyro-beam, the storey and gyro can be shown as follows [8];

$$\omega_1 = \sqrt{\frac{C_4}{C_1 + G_5^2 (I_o + I_{fx})}} \quad (8)$$

$$\omega_2 = \sqrt{\frac{C_{11}}{C_8 + G_{15}^2 (I_o + I_{fx})}} \quad (9)$$

$$\omega_g = \sqrt{\frac{m_f g R + k_g}{I_o + I_{fx}}} \quad (10)$$

## 2.2. Model Test Set-Up

The experimental model set-up is given in Figure 4 and the physical parameters of the test model are representing in Table 1. The primary structure is a solid rectangular aluminium block supported by 1 mm thick 25 mm wide four steel spring beams. The gyroscopic vibration absorber also consists of electric motor (1800Kv / 875w NTM Prop Drive Series 35-36A), which is remotely controlled with a

radio control system (FlySky FS-T6B), mounted in a gimbal by assembling to the free end of a vertical cantilever column. This gyro carrier beam is attached to the base of the primary mass by a rigid clamp for researching the horizontal and vertical displacements. The base of the model is restrained to horizontal motion by the use of four bearings moving on a smooth flat surface. The sinusoidal displacement is horizontally applied to the base of the main structure via a rigid joint.

A vibration test system (Brüel & Kjaer / LDS Comet USB ) was used to sweep the frequency responses of the one-story building by the channel of multiple mode (SCO-02V-01) and tracking filters (SCO-02V-02). The shaker control system consists of two primary components: (1) the hardware and (2) Windows-based application software. The shaker control system performs data measurement and drive signal generation. The signal rides a 311 N electrodynamic shaker (LDS V450). The shaker system can provide for varying amplitudes and frequencies of excitation. The shaker operates between the frequency range of 1.2 to 7500 Hz from either a sine wave or random signal input. V450 shaker is driven by the ling dynamic systems (PA500L amplifier). The V450 model is fitted with a low impedance armature, which is suited for use with the PA500L amplifier. During the experiments, the computer was used to store, display, and analyze experimental data.

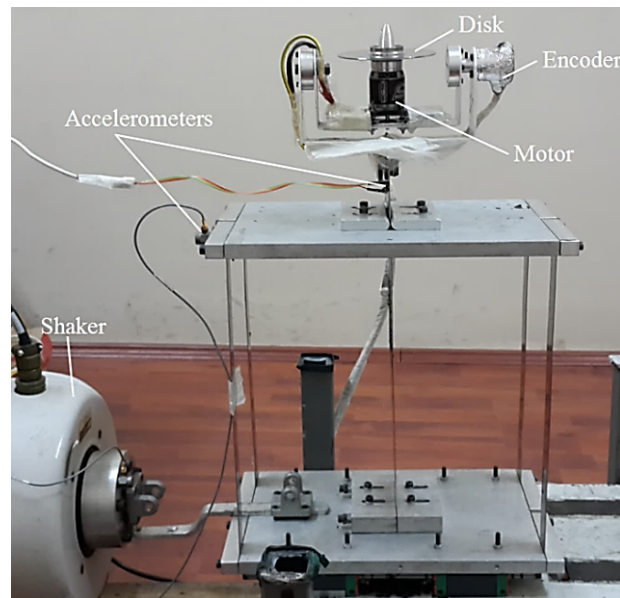


Figure 4. Experimental model of the cantilever model with the one-story building and gyroscope [8]

For the sinusoidal excitation experiments, the accelerometers were used as transducers to monitor the displacement response of the one-story building and the gyroscope carrier beam (Figure 4). One accelerometer (3-Axis Accelerometer - MMA7341L) was attached to the gyro carrier beam of the gyroscopic vibration absorber, while the other one (DeltaTron accelerometers - Type 4513) was attached to the top table of the primary mass. An accelerometer (DeltaTron accelerometers - Type 4513) was stuck to the table of the shaker to monitor its motion to send a feedback signal to the vibration controller of the output signal of the shaker. The signals from the accelerometers on the primary structure and absorber, and the accelerometer on the shaker were fed into the data acquisition and analysis system. Additionally, an incremental encoder (RI 30-O) was mounted onto the gyroscope to measure the signal of the angular motion of the gimbal.

### 3. Results and Discussion

#### 3.1. Theoretical Results

In order to obtain the optimum operating conditions, the investigations are carried out with the different frequency ratios of the one-story building, but the frequency ( $\omega_2$ ) of the one-story building has been considered to be constant in the system. The gyro has been shaped with  $\omega_g = \omega_2$ ,  $\omega_g = 1.2\omega_2$ , and  $\omega_g = 2\omega_2$ , respectively. Here, natural frequency of one story building  $\omega_2$  and natural frequency of the gyro  $\omega_g$ . As seen from the response curves for these frequency ratios by the base excitation of  $z=$

$z_0 \cos(\omega t)$  in Figures 5-7, the ratio of  $\omega_g = 1.2\omega_2$  is more effective throughout the varying rotor speeds. The tip displacement of the storey can be fairly decreased if the angular momentum is  $L_\Omega = 0.0660 \text{ kg.m}^2/\text{s}$  at  $\Omega = 4000 \text{ rpm}$ . So, the optimal performance was achieved at the ratio of  $\omega_g = 1.2\omega_2$  with  $\Omega = 4000 \text{ rpm}$  which generated less displacement by comparison.

Consequently, throughout the next entire analysis the height of the one-story building model for  $\omega_g = 1.2\omega_2$  with an optimum angular momentum ( $L_\Omega = 0.0660 \text{ kg.m}^2/\text{s}$ ) is preferred as an optimum frequency ratio.

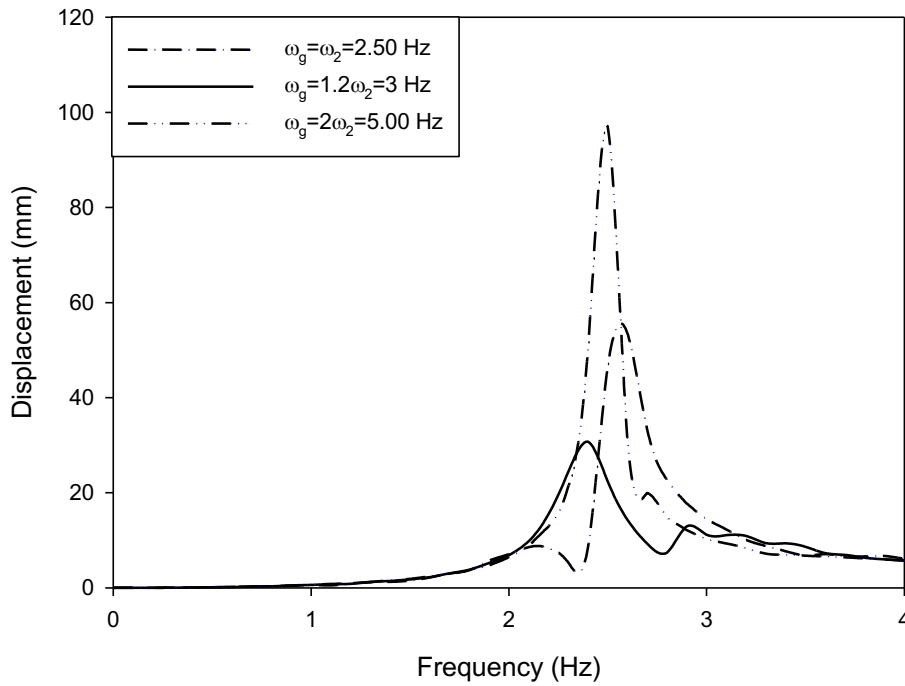


Figure 5. Theoretical response curves for varying frequency ratios by the base excitation of  $z = z_0 \cos(\omega t)$ . ( $\Omega = 2000 \text{ rpm}$ ,  $\omega_2 = 2.5 \text{ Hz}$ ,  $\omega_1 = 7.5 \text{ Hz}$ ,  $z_0 = 5 \text{ mm}$ ,  $m = 0.069 \text{ kg}$ ) [8]

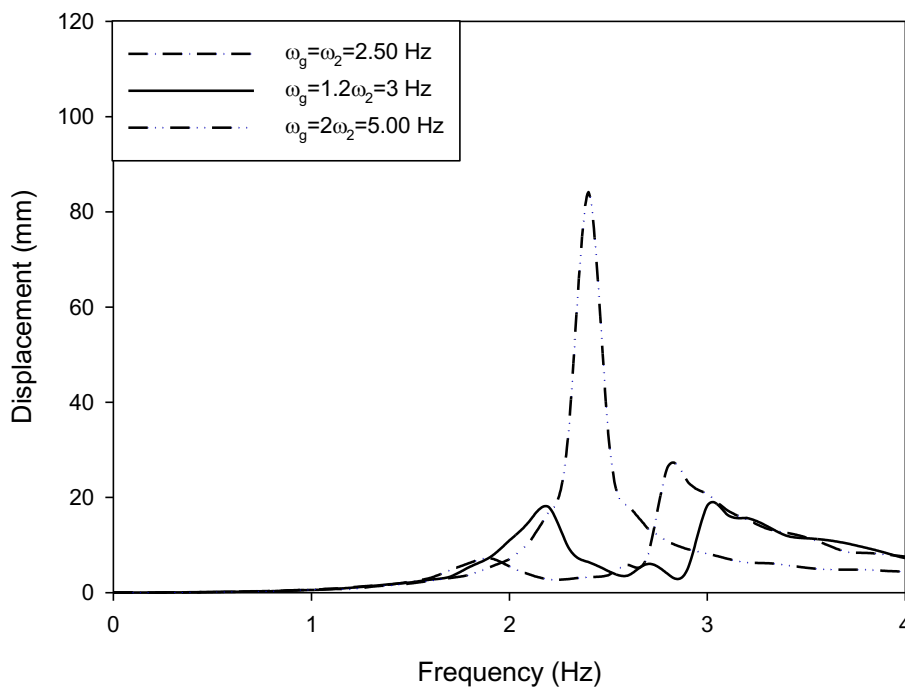


Figure 6. Theoretical response curves for varying frequency ratios by the base excitation of  $z = z_0 \cos(\omega t)$ . ( $\Omega = 4000 \text{ rpm}$ ,  $\omega_2 = 2.5 \text{ Hz}$ ,  $\omega_1 = 7.5 \text{ Hz}$ ,  $z_0 = 5 \text{ mm}$ ,  $m = 0.069 \text{ kg}$ ) [8]

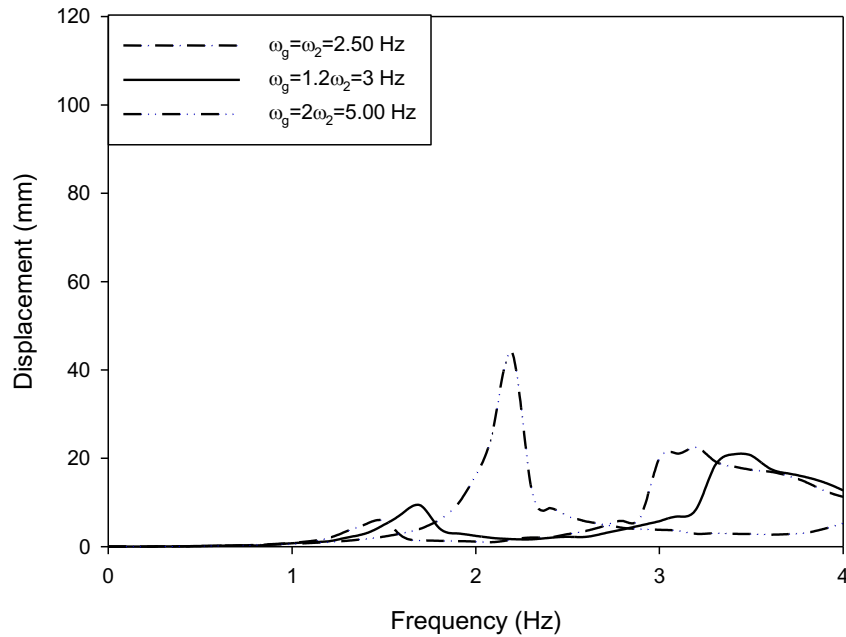


Figure 7. Theoretical response curves for varying frequency ratios by the base excitation of  $z = z_0 \cos(\omega t)$ . ( $\Omega = 8000$  rpm,  $\omega_2 = 2.5$  Hz,  $\omega_1 = 7.5$  Hz,  $z_0 = 5$  mm,  $m = 0.069$  kg) [8]

### 3.2. Experimental Results for the Frequency Ratio, $\omega_g = 1.2\omega_2$ of the One-Story Building

#### 3.2.1. Results for different disk masses (m)

By the base excitation of  $z = z_0 \cos(\omega t)$ , Figure 8 represents frequency scan of the displacement curves of the one-storey building for varying disk masses (m) of gyro. It can be seen that tip responses of the one-storey building is slightly changed within range of  $m = 0.023$ - $0.115$  kg. So the inertia on the frequency response can be ignored for this range of disk mass with  $\Omega = 0$  rpm.

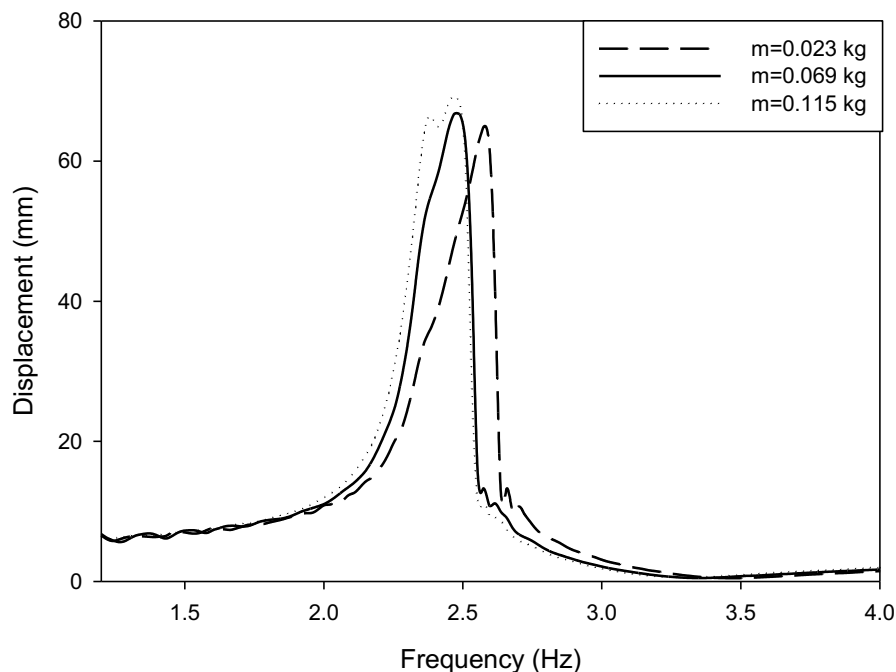


Figure 8. Frequency sweep curves of the one-storey building for varying disk masses (m) by the base excitation of  $z = z_0 \cos(\omega t)$ . ( $z_0 = 5$  mm,  $\Omega = 0$  rpm and  $\omega_g = 1.2\omega_2$ ) [8]

Figures 9 and 10 show the frequency scan for varying disk masses (m) of case  $\Omega = 3000$  rpm. It presented that the displacement amplitude is reduced by increasing the disk mass at the first resonant

frequency mode. However, there is the existence of two vibration peaks outside the first mode frequency. These peaks move towards opposing frequency directions. The amplitude of one peak by low frequency decreases when the other peak increases as the disk mass increased. Up to a value of disk mass there is significantly suppression in the vibration. But beyond this, as the disk mass is increased, the reduction of the vibration is slightly changed. Similar change in sweep pattern is also observed changing disk speed as shown in Figures 11-12.

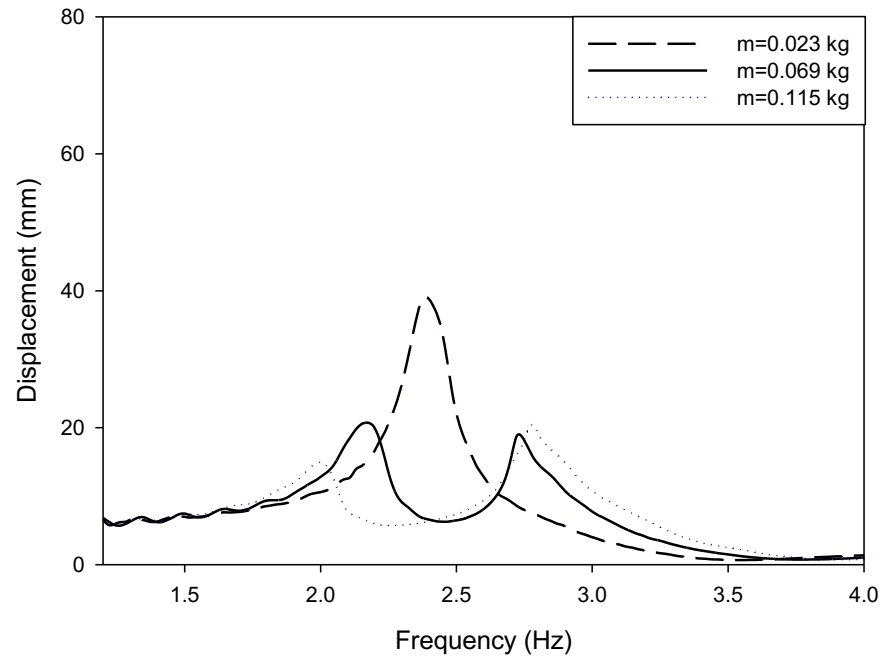


Figure 9. Frequency sweep curves of the one-storey building for varying disk masses (m) by the base excitation of  $z = z_0 \cos(\omega t)$ . ( $z_0 = 5 \text{ mm}$ ,  $\Omega = 3000 \text{ rpm}$  and  $\omega_g = 1.2\omega_2$ ) [8]

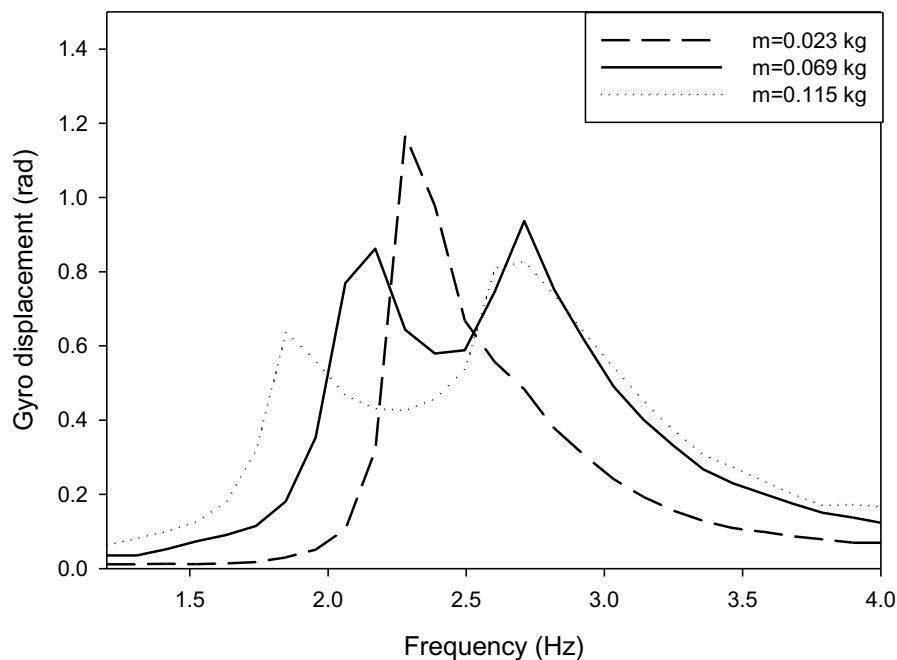


Figure 10. Frequency sweep curves of gyroscope for varying disk masses (m) by the base excitation of  $z = z_0 \cos(\omega t)$ . ( $z_0 = 5 \text{ mm}$ ,  $\Omega = 3000 \text{ rpm}$ ,  $\omega_g = 1.2\omega_2$ ) [8]

### 3.2.2. Results for different disk speeds ( $\Omega$ ) of gyro

Figures 11-12 show the frequency sweep displacements for varying disk speeds ( $\Omega$ ) for case  $m = 0.069 \text{ kg}$ . The gyro-beam system has significantly reduced the displacement as we increase the disk speed. The existence of two vibration peaks which move towards opposing frequency directions is found to

decrease the amplitude of displacement compared to the other peak as the disk speed is increased. So, the intersection of these peaks (at  $\omega=2.10$  Hz and  $\omega=2.85$  Hz) as seen in Figure 13 results in optimum disk speed of gyro. Up to this value there is significantly suppression in the vibration at  $\omega=2.45$  Hz. But beyond this, as the disk speed is increased, the vibration at  $\omega=2.85$  Hz is increased compared to the other peaks. So, the displacement amplitude of the story can be considerably decreased when the angular momentum is  $L_\Omega=0.0660$  kg.m<sup>2</sup>/s at  $\Omega = 4000$  rpm.

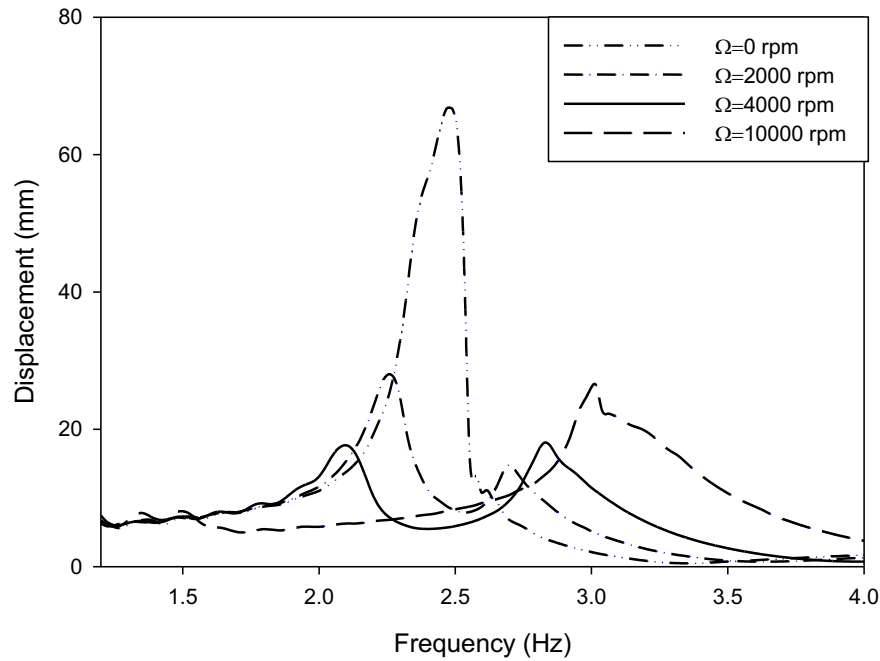


Figure 11. Frequency sweep curves of the one-storey building for varying disk speeds ( $\Omega$ ) by the base excitation of  $z= z_0\cos(\omega t)$ . ( $z_0=5$  mm,  $m=0.069$  kg and  $\omega_g = 1.2\omega_2$ ) [8]

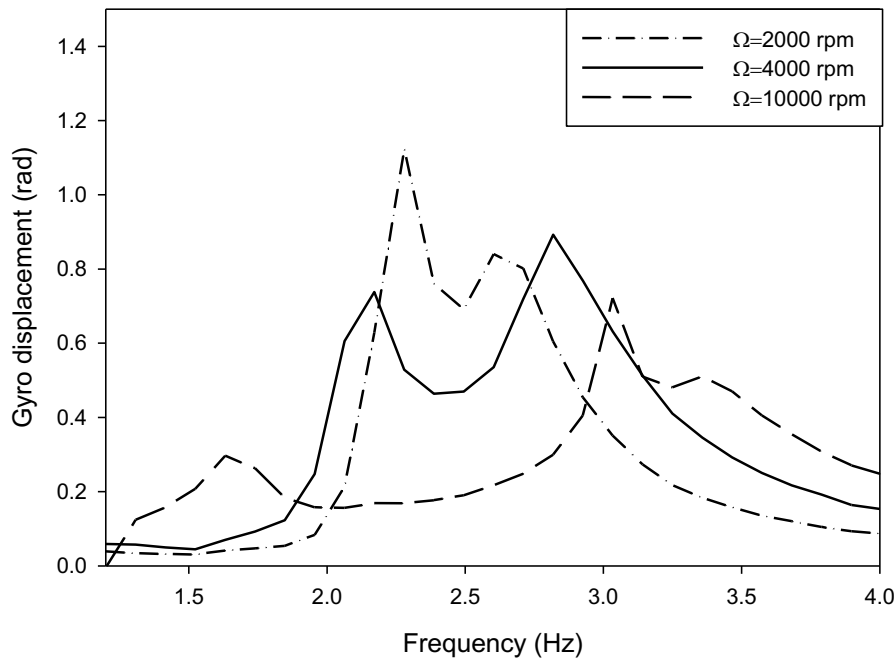


Figure 12. Frequency sweep curves of gyroscope for varying disk speeds ( $\Omega$ ) by the base excitation of  $z= z_0\cos(\omega t)$ . ( $z_0=5$  mm,  $m=0.069$  kg and  $\omega_g = 1.2\omega_2$ ) [8]

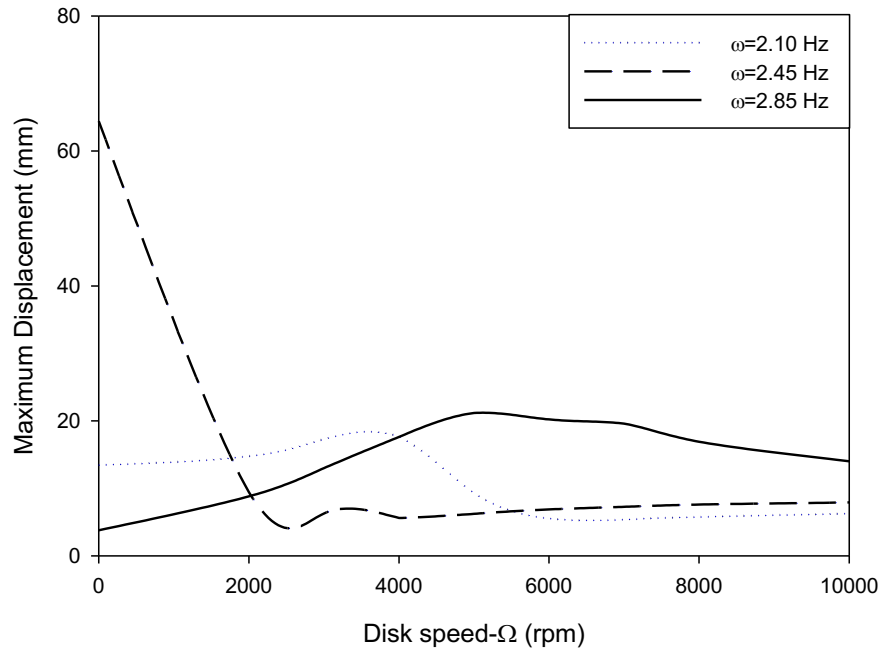


Figure 13. Disk speed response curves of the one-storey building for different base excitation frequency ( $\omega$ ) with  $z= z_0\cos(\omega t)$ . ( $z_0=5$  mm,  $m=0.069$  kg and  $\omega_g = 1.2\omega_2$ ) [8]

### 3.2.3. Instantaneous results when the gyroscope is suddenly activated

Figure 14 represents the frequency response curves of different excitation frequencies ( $\omega$ ) with the base excitation of  $z= z_0\cos(\omega t)$ . Instantaneous activation of gyroscope on the one-storey building is experimentally investigated. At the different excitation frequencies, the electric motor is remotely activated to the disk speed  $\Omega=4000$  rpm with the radio control system. As seen in Figure 14, the vibration is reduced from the tip displacement almost to the amplitude of base excitation within 6 seconds when the gyroscope is suddenly activated at about the maximum displacement of the one-storey building.

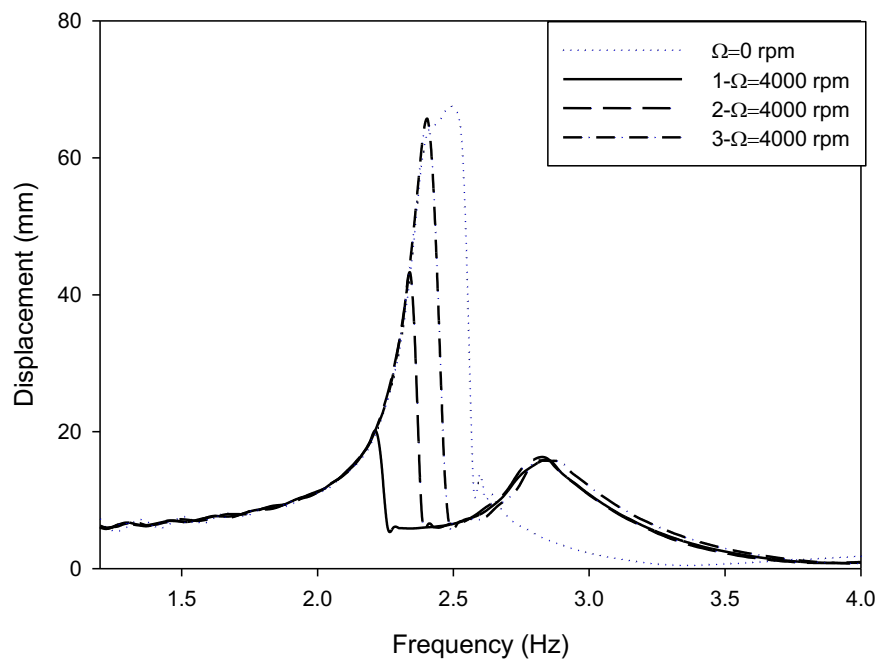


Figure 14. Experimental frequency response curves of the one-storey building for the instantaneous activation of gyroscope. No active (dotted), active after  $\omega=2.20$  Hz (solid),  $\omega=2.35$  Hz (dashed) and  $\omega=2.44$  Hz (dash-dot). ( $z_0=5$  mm,  $m=0.069$  kg and  $\omega_g = 1.2\omega_2$ ) [8]

## 4. Conclusion

In order to maintain the optimal damper effect of the gyroscope, the disk speed decreased with increasing disk mass. If the disk mass was 0.069 kg, the optimum disk speed was around 4000 rpm, while increasing the disk mass to 0.115 kg the optimum disk speed decreased to 3000 rpm. Since low mass and volume are preferred in dampers, the mass of the gyroscope can be decreased if the speed of disk is increased as much as possible according to the engine capacity.

The best damping in the first mode occurred at the angular momentum of the disk for  $L_{\Omega} = 0.0660$  kg.m<sup>2</sup>/s. It has been observed that the best energy transfer (damping) according to this angular momentum is realized at the frequency ratio of  $\omega_{gyro} / \omega_{building} = 1.2$ . Control moment gyroscope has a superior advantage over conventional vibration dampers. So the gyro-column is efficient on a wide frequency range from the frequency of the gyro to the frequency of the building resonance by using an adjustable angular momentum of a gyroscope.

The initially stationary disk is accelerated suddenly at  $\Omega = 4000$  rpm for angular momentum  $L_{\Omega} = 0.0660$  kg.m<sup>2</sup>/s, thereby quickly minimizing the displacement of the structure in the first mode. This experiment shows that when the structure starts to oscillate as a result of an earthquake or any external factor, the vibration amplitudes of the structure can be quickly minimized by activating the disk.

An active gyro with a proportional controller can reduce the random vibration amplitude of seismic responses of a building. For subsequent research, the gimbal of the gyro can be guided by a torque control loop using a measured precession of the gimbal fed back to the control unit, which creates the counter-reactionless moment needed to stabilize the building in the upright position.

## Acknowledgment

This research is supported in part by the Scientific and Technological Research Council of Türkiye (TÜBİTAK) via grant number 114M760.

## Conflict of Interest Statement

The authors declare that there is no conflict of interest

## References

- [1] F. Ünker, "Tuned gyro-pendulum stabilizer for control of vibrations in structures," *Int. J. Acoust. Vib.*, vol. 25, no. 3, pp. 355–362, 2020. doi:10.20855/ijav.2020.25.31632
- [2] T. T. Soong, G. F. Dargush, *Passive Energy Dissipation Systems in Structural Engineering*. New York: John Wiley and Sons, 1997.
- [3] T. T. Soong and B. F. Spencer, "Supplemental energy dissipation: state-of-the-art and state-of-the-practice," *Eng. Struct.*, 2002, doi:10.1016/S0141-0296(01)00092-X
- [4] M. P. Singh, E. E. Matheu, and L. E. Suarez, "Active and semi-active control of structures under seismic excitation," *Earthq. Eng. Struct. Dyn.*, 1997. doi:10.1002/(SICI)1096-9845(199702)26:2<193::AID-EQE634>3.0.CO;2-#
- [5] F. Ünker and O. Çuvalcı, "Seismic Motion Control of a Column Using a Gyroscope," *Procedia - Soc. Behav. Sci.*, vol. 195, pp. 2316–2325, Jul. 2015. doi:10.1016/J.SBSPRO.2015.06.183
- [6] O. Çuvalcı, F. Ünker, T. Batuhan Baturalp, U. Gülbulak, and A. Ertaş, "Modal Control of Cantilever Beam Using a Gyrostabilizer," *Sound&Vibration*, vol. 55, no. 4, pp. 281–294, 2021. doi:10.32604/sv.2021.015705
- [7] F. Ünker and O. Çuvalcı, "Optimum Tuning of a Gyroscopic Vibration Absorber Using Coupled Gyroscopes for Vibration Control of a Vertical Cantilever Beam," *Shock Vib.*, vol. 2016, pp. 1–10, 2016. doi:10.1155/2016/1496727
- [8] F. Ünker, "Vibration control in structures with gyroscope," Karadeniz Technical University, 2018.
- [9] F. Ünker, "Proportional control moment gyroscope for two-wheeled self-balancing robot," *J. Vib. Control*, vol. 28, no 17–18, pp. 2310–2318, Sep. 2022. doi:10.1177/10775463211009988
- [10] F. Ünker, "Angular Momentum Control for Preventing Rollover of a Heavy Vehicle," *Int. J. Automot. Sci. Technol.*, pp. 135–140, Jun. 2022. doi:10.30939/ijastech..1085111

- [11] F. Ünker, "Oscillation Control of Two-Wheeled Robot using a Gyro Stabilizer," *Gazi Üniversitesi Fen Bilim. Derg. Part C Tasarım ve Teknol.*, Jun. 2022. doi:10.29109/gujsc.1062497
- [12] M. Soleymani and M. Norouzi, "Active gyroscopic stabilizer to mitigate vibration in a multimegawatt wind turbine," *Wind Energy*, vol. 24, no. 7, pp. 720–736, Jul. 2021. doi:10.1002/we.2599
- [13] S. F. Ali and R. Padhi, "Active vibration suppression of non-linear beams using optimal dynamic inversion," *Proc. Inst. Mech. Eng. Part I J. Syst. Control Eng.*, vol. 223, no. 5, pp. 657–672, 2009. doi:10.1243/09596518JSC688
- [14] A. H. Nayfeh and P. F. Pai, *Linear and nonlinear structural mechanics*, vol. 40, no. 2. New Jersey: Wiley Interscience, 2004. doi:10.1007/s11012-005-0327-y
- [15] L. D. Zavodney and A. H. Nayfeh, "The non-linear response of a slender beam carrying a lumped mass to a principal parametric excitation: Theory and experiment," *Int. J. Non. Linear. Mech.*, vol. 24, no. 2, pp. 105–125, Jan. 1989. doi:10.1016/0020-7462(89)90003-6
- [16] E. Esmailzadeh and G. Nakhaie-Jazar, "Periodic behavior of a cantilever beam with end mass subjected to harmonic base excitation," *Int. J. Non. Linear. Mech.*, vol. 33, no. 4, pp. 567–577, Jul. 1998. doi:10.1016/S0020-7462(97)00038-3

This is an open access article under the CC-BY license

